Mapping birefringence in three dimensions using polarized light field microscopy: the case of the juvenile clamshell

Mai Thi Tran and Rudolf Oldenbourg
Marine Biological Laboratory, Woods Hole, MA 02543, USA, and
Physics Department, Brown University, Providence, RI 02912, USA

Contact information:
Mai T Tran, PhD
Marine Biological Laboratory
7 MBL Street
Woods Hole MA 02543
Tel.: +1-508-289-7426
email: mtran@mbl.edu

Key words: Light field microscope, LC-PolScope, Clamshell, Biaxial crystal, Polarized light field microscope, Birefringence.

ABSTRACT

We report methods to generate three dimensional maps of birefringence, its position and orientation in juvenile shells of the Atlantic hard clamshell (*Mercenaria mercenaria*). For measuring the retardance and optic axis orientation of curved shell surfaces in three dimensions, we developed enhanced acquisition and processing algorithms and combined results from conventional and light field imaging approaches to reconstruct the three dimensional shell shape and its anisotropic optical properties. Our work represents the first successful attempt to generate such maps at a spatial resolution of about 2 μm and angular steps of about 9° in terms of the inclination angles of the optic axis. The maps of clamshell birefringence provide structural insights into the early mineralization during juvenile clamshell development.

1. INTRODUCTION

Recently, we combined light field imaging and the liquid crystal based polarized light microscope (LC-PolScope) into the light field LC-PolScope that combines both orthoscopic and conoscopic observations into a single measurement process. In a first application we analyzed the birefringence of thin stratified films of polycrystalline calcite [Oldenbourg, 2008]. Building on these results, we are now extending the technique to observe and analyze the three dimensional geometric shape and optical properties of juvenile shells of the Atlantic hard clamshell, *Mercenaria mercenaria*, a thicker and more complex shape than a thin, stratified film.

The shells of bivalve mollusks like the hard clamshell are composed of calcium carbonate crystals in the form of calcite and/or aragonite, both of which exhibit strong birefringence. Juvenile shells of *M. mercenaria*, 2 to 4 days after fertilization, resemble a bent, thin, crystalline sheet, in which the orientation of the optic axis of the underlying crystal structure varies systematically with the position in the sheet (Tiwari and Gallager, 2003). Hence, these juvenile shells represent a birefringent structure that is well suited to further develop polarized light field imaging. Our results also provide benchmark and analysis approaches that relate optical properties of juvenile shells to their morphology that can be exploited for monitoring the health and development of bivalve aquacultures.

In the following sections we describe the microscopes used and the methods to clean, prepare and manipulate samples, including epitaxial crystal growth to reveal the morphology and orientation of calcium carbonate crystals inside the shells. The epitaxial crystal growth is examined by Scanning Electron Microscopy (SEM), and the

3D shape of cleaned shells is reconstructed by two different methods, conventional bright field microscopy and light field microscopy. The polarized light analysis using the light field LC-PolScope reveals the optical anisotropy and 3D orientation of its optic axis and their relationship to the morphology of the shell. Finally, the new light field LC-PolScope is applied to estimate the shell's thickness and its relationship to the shell's age. The results are compared with measurements using traditional techniques.

2. MATERIALS AND METHODS

2.1 Preparation of shells for microscopy

In our experiments, we examined three-day old hard clam embryos from the Aquacultural Research Corporation (ARC hatchery) in Dennis, Massachusetts. First, a batch of embryos were fixed with 2% formalin (Fisher Scientific). Then the batches were transferred to 10%, 30%, 50% and 70% Ethanol, consecutively, rinsed with deionized water ten times, and soaked for six hours in 8.25% sodium hypochloride (NaClO) bleach solution to remove organic materials. Finally, the larval shells were washed ten times in deionized water and stored in 70% Ethanol.

For microscopic observations, a small amount of shells, which had collected in the bottom precipitate, was transferred onto a coverslip and left to dry completely.

For imaging in the scanning electron microscope, the dried shells were either covered with a thin platinum film, or placed directly into the SEM sample chamber without a conducting layer. For optical microscopy, the dried shells were immersed in oil (n_{medium} =1.52) and sandwiched between a microscope slide and a coverslip and sealed with nail polish.

2.2 Epitaxial crystal growth on juvenile clamshells

After fixing and removing organic materials, a small batch of shells was suspended for three days in MBL artificial seawater with saturated sodium bicarbonate ($NaHCO_3$) to promote the epitaxial growth of calcium carbonate crystals on the shells' surface. The treated shells were washed many times with distilled water and were dehydrated overnight for SEM imaging.

2.3 Light field LC-PolScope

A bright field microscope and polarized light microscope such as the LC-PolScope can be easily converted into isotropic and polarized light field microscopes by exchanging the regular camera with a light field camera [Levoy, 2006]. In the light field camera, there is a microlens array, which is placed at the image plane of the main lens, while the traditional detector array is placed in the focal plane 2.5 mm behind the microlens array. This microlens array allows the sensor to record additional information about the incoming rays of light, including their intensities and directions.

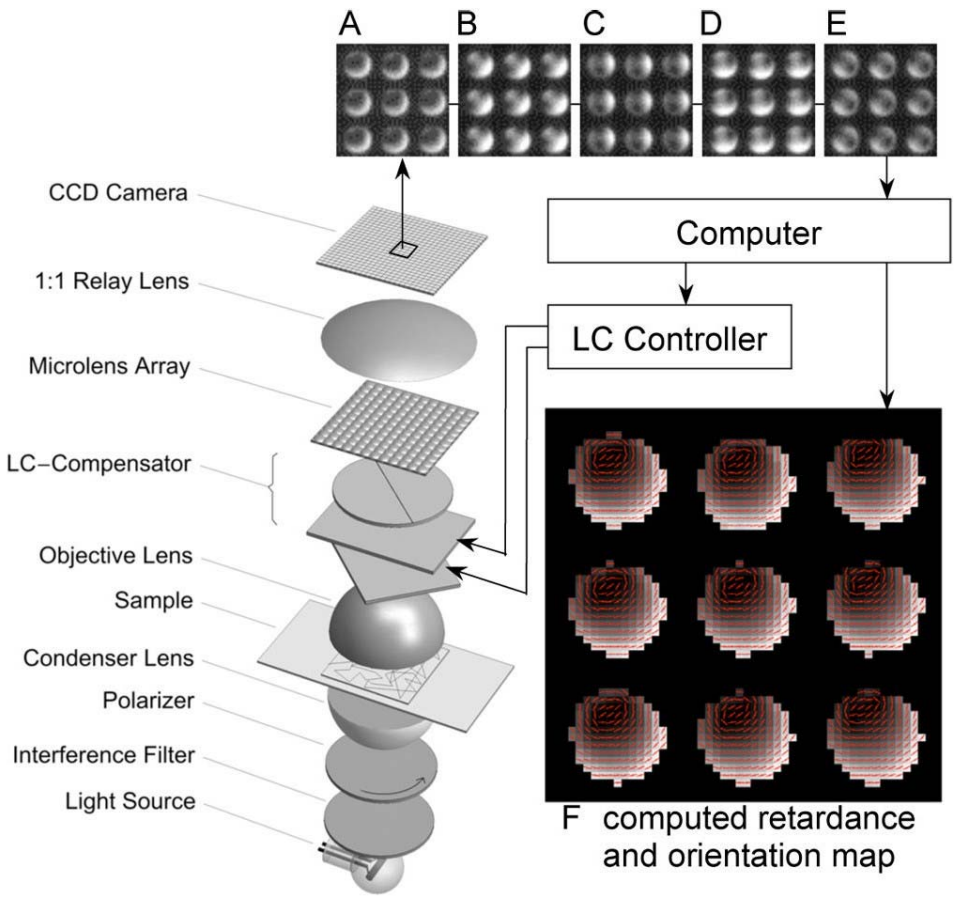

Figure 1: Schematic of light field LC-PolScope including the optical setup, image acquisition and processing components. The optical parts include the light source, interference band pass filter, left circular polarizer, condenser lens, sample, objective lens, universal compensator, microlens array (placed in the objective lens' image plane), and a 1:1 relay lens. (**A-E**) Complete analysis of the polarized light field requires 5 raw images, corresponding to five settings of the LC compensator. The computer synchronizes the raw image acquisition with the compensator settings using a serial connection to the liquid crystal controller. (**F**) Based on the raw intensity images, the computer calculates a retardance and an orientation map, shown here as a composite image with red lines indicating the slow axis orientation. Reprinted from Oldenbourg et al., 2008.

In our prototype, shown as a schematic in **Figure 1**, the universal compensator was fabricated by Meadowlark Optics Inc. (Frederick, CO). The microlens array of the light field camera has a 125 μm pitch and consists of square microlenses with a focal length of 2.5 mm (Adaptive Optics Associates, now Northrop Grumman Mission Systems, Cambridge, MA). The back focal plane of the microlens array is projected by a 1:1 relay lens onto a 2048x2048 pixel monochrome CCD camera (Retiga, 4000R, QImaging, Surrey BC, Canada, the size of a pixel is 7.4 x 7.4 μm). The relay lens was put together from two AF Nikkor 50 mm f/1.4D lenses (Nikon, Melville, NY). The relay lens conveniently increases the required space between the microlens array and the camera sensor, which enables an easy conversion between conventional camera and light field camera.

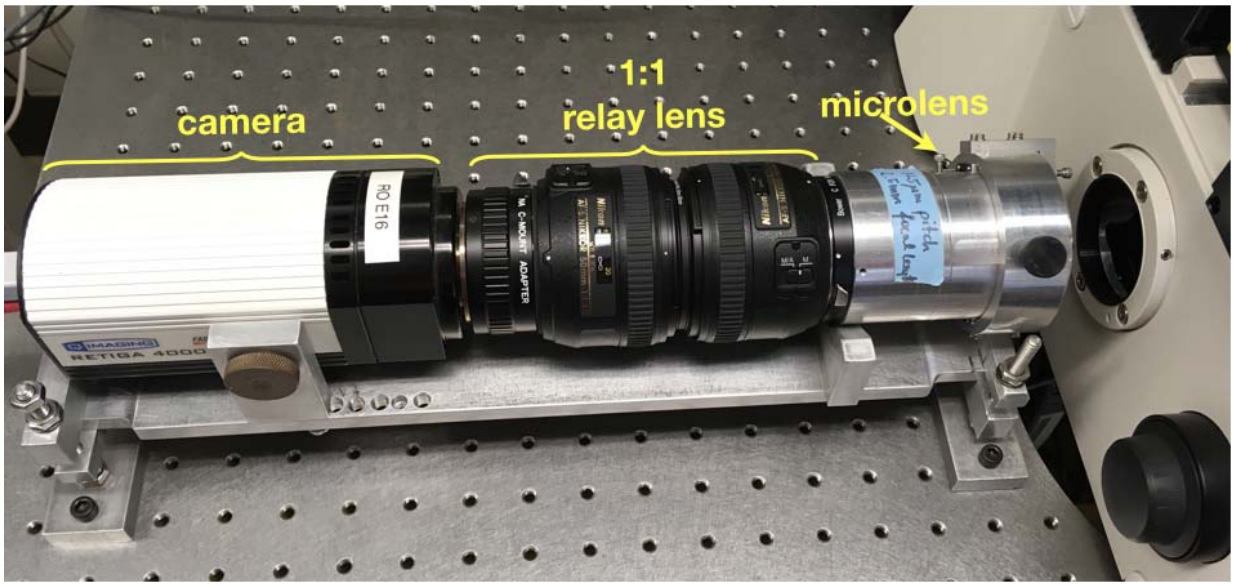

Figure 2: The light field camera includes a microlens array at the image plane, a 1:1 relay lens and conventional CCD camera (QImaging Retiga 4000R).

3. RESULTS

3.1 Three dimensional shape reconstruction

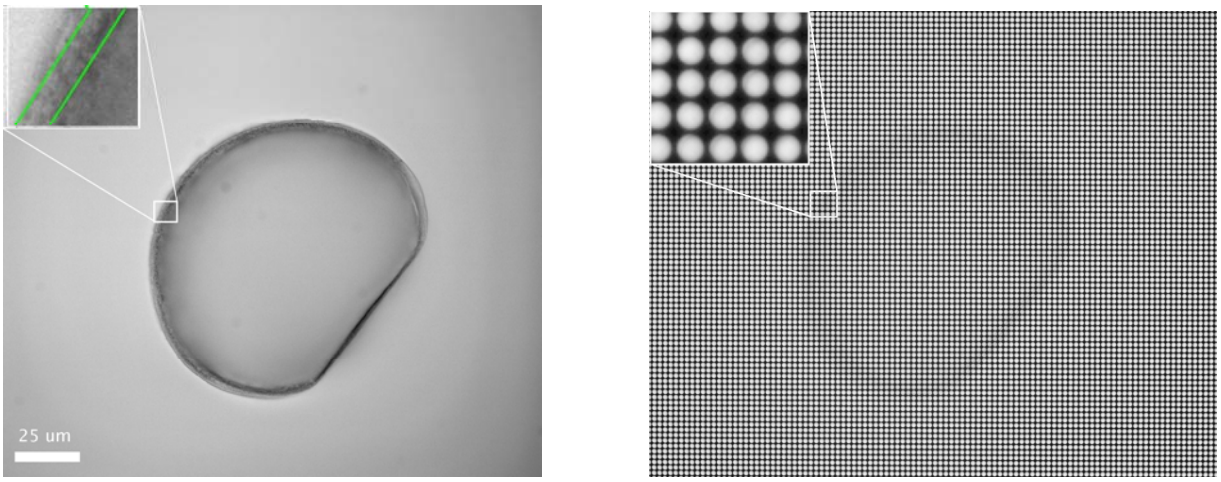

(**A**) (**B**)

Figure 3: Images of a three-day old clamshell recorded with a bright field microscope equipped with a 60x/1.4 NA objective lens and matching condenser optics, and (**A**) a conventional camera (Hamamatsu ORCA Flash4.0) or (**B**) a light field camera (specs described in section 2.3). The shell partially absorbs and scatters the light that passes through it and its image appears dark against a bright background. The inset in (**A**) shows a magnified and contrast enhanced portion of the shell, with two green lines drawn by hand to identify the outer and inner surface of the shell. The inset in (**B**) is an enlarged portion showing the intensity behind 5x5 microlenses with applied contrast enhancement.

In a first step towards mapping the 3D optical anisotropy of hard clamshells, we reconstructed the 3D shape of the shell using a bright field microscope setup without any polarizing components. In this paper, two methods were applied to build up a three dimensional model of the shell. First, the traditional method uses a bright field microscope and a conventional camera to image the absorption or attenuation of light that has passed through the shell. Since the hard clamshell material absorbs and scatters light, its shape can be reconstructed from a series of focal sections using high

resolution optics (**Fig. 3A**). In doing so, we neglected the small mismatch in refractive index between the oil (n=1.52) that surrounds the shell and the shell material (n_o=1.53, n_e=1.68). Assuming an average refractive index mismatch of 0.1, we underestimated the thickness of the shell by about 4%. Hence, we ignored this refraction effect. By identifying the shell's outer and inner surface in each slice by visual inspection (**Fig. 4A)**, a model of the shell can be drawn and even 3D printed (**Fig. 5D**). Second, while using the same optical setup, we replaced the conventional camera with a light field camera to capture the shell's three dimensional distribution of absorption/scattering centers in a single snapshot (**Fig. 3B**). This light field image needs to be processed further to create optical sections or different perspective views of the shell. Here, the deconvolution method described in (Broxton et at., 2013) was utilized to reconstruct a 3D model of the shell from its light field image.

Figure 4 illustrates reconstructed cross sections, which correspond to optical sections through the shell recorded at different focal planes (z-sections) and comparing corresponding z-sections obtained by conventional, high resolution bright field imaging (**Fig. 4A**) and by deconvolving the light field image (**Fig. 3B**). Each conventional optical section contains image details at high spatial frequencies that represent the shell's cross section at that focal plane, as pointed out by the green outline in the right most panel of **Figure 4A**. Blurred image features outside the outlined cross section that appear as a black ring represent shell portions that are out of focus. Depending on the optical section, out of focus features can be more dominant in the image than the subtle, but detailed in focus features. In contrast, the optical sections reconstructed from the light field image don't contain fine absorption details from inside the cross

section, but present the in focus part of the shell's cross section at lower resolution without dominant out of focus features. Hence, as expected, while the light field method does not have as good an in focus resolution as traditional imaging, this method paired with proper deconvolution largely removes out of focus features and allows the reconstruction of the 3D shape of the shell. Moreover, with light field imaging we can reconstruct the entire volume by recording a single image without moving the stage or specimen. Therefore, the method will be advantageous when analyzing dynamic scenes.

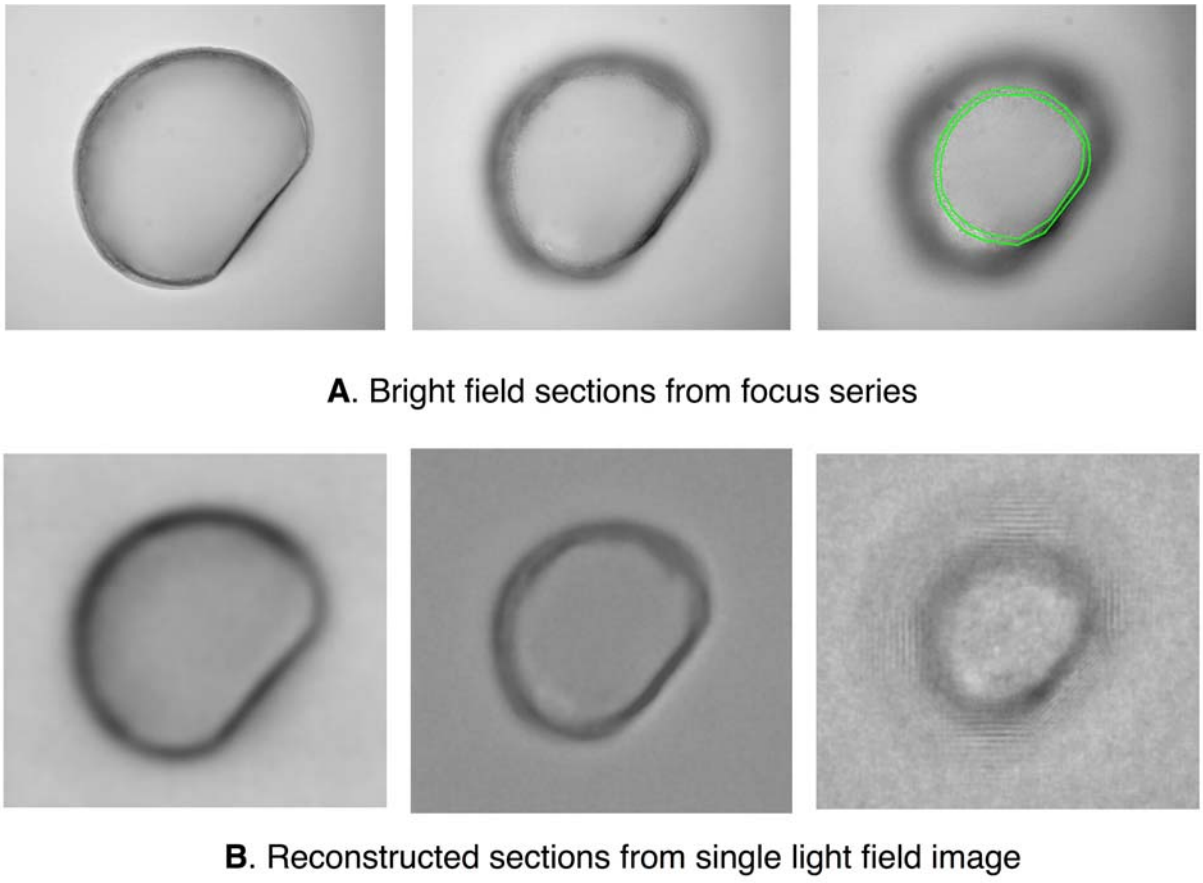

Figure 4: (**A**) Optical sections through the juvenile clamshell of **Fig. 3A** recorded with the bright field microscope and conventional camera. The green lines drawn by hand in the right most panel outline the fine absorption details that define the shell's cross section at that focus plane (see main text). Note that

the dark ring outside the green outline represents out of focus information and not the shell's cross section at that focus plane. (**B**) Optical sections reconstructed from a single light field image (**Fig. 3B**) of the shell using the deconvolution method of Broxton et al. (2013). Due to the rectification step in the deconvolution method, the shell is rotated by a small angle. The optical sections reconstructed from the light field image do not contain fine absorption details from inside the cross section, but present the in focus part of the shell's cross section at lower resolution without dominant out of focus features. Light field imaging trades some lateral resolution for axial resolution and the ability to reconstruct the 3D shape of the shell.

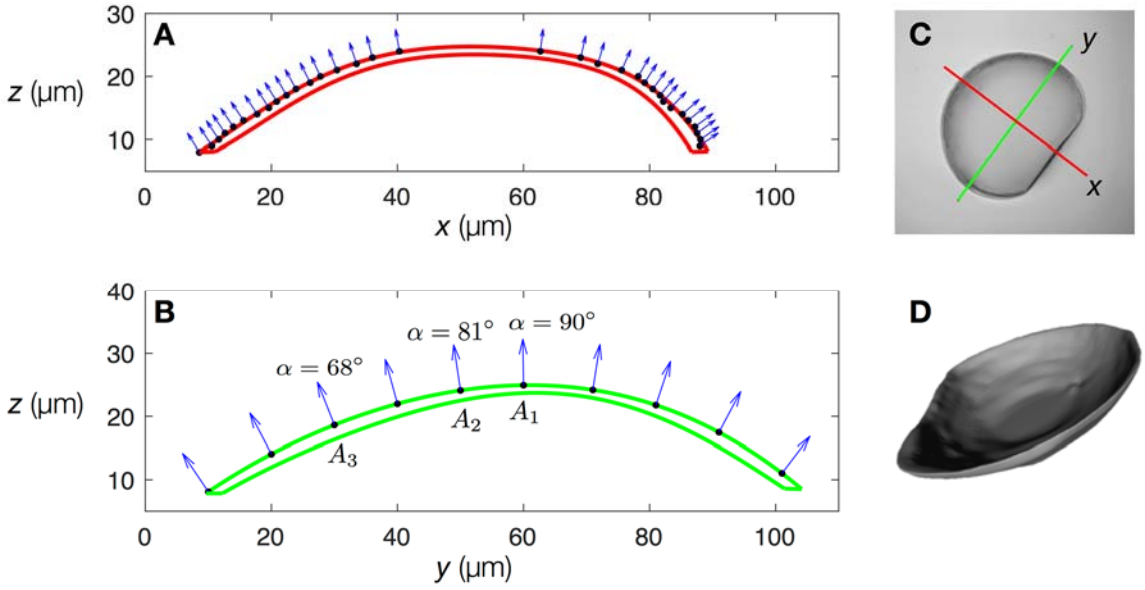

Figure 5: (A, B) Two vertical cross sections through the shell of **Fig**. **3A**, reconstructed using the complete focus series recorded with the conventional camera. The plane of the cross section is indicated by the green and red line in (**C**) and includes in both cases the microscope axis, which runs vertical in (**A**) and (**B**). The blue arrows in (**A**) and (**B**) are normal to the shell surface, α is the inclination angle of the normal. Points A_1 and A_3 indicate locations of micro lenses that are further examined in **Fig.10**. (**D**): 3D printable model of three-day old juvenile clamshell reconstructed from light microscopy data.

The series of optical sections can be used to reconstruct the inner and outer shell surface and calculate the normal angles and thickness of the shell. In **Figure 5**, two vertical cross sections are shown in panels **A** and **B**, reconstructed from optical sections that were sliced along the green and red lines in **Figure 5C**. The blue arrows present the normal vectors at points of the shell's surface. In particular, the thickness of the shell parallel to its normal is calculated by the product of the thickness retrieved from the horizontal optical sections and the cosine of the normal angle. For example, the cross section near the top plane of the shell is shown in **Figure 6**, where the normal of the shell is inclined by 81° to the focus plane, as determined in **Figure 5B**. Using the edge detection function in ImageJ, we found the in focus edges of the shell and measured the projected thickness as 3792 ± 108 nm. The uncertainty of the measurement comes from the size of one pixel. So the thickness at the top plane of the shell is: T = 3792nm* cos(81°) = 593 ± 20 nm.

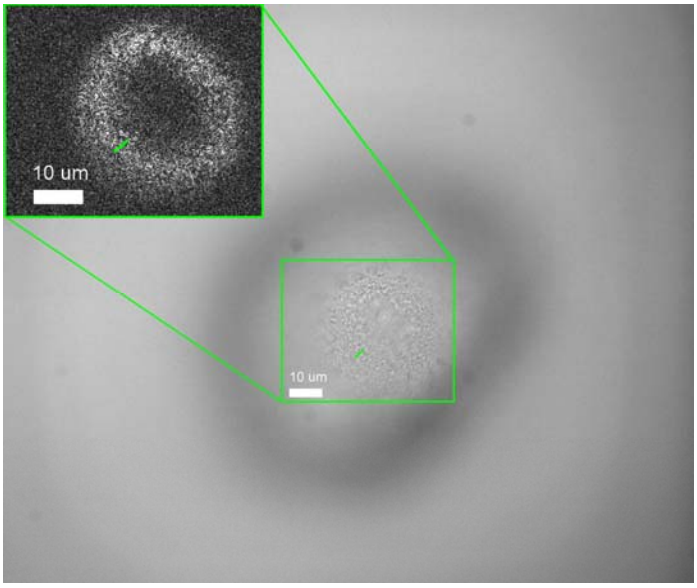

Figure 6: Conventional bright field image of the shell at a focus plane close to its top. (Inset) The shell cross section was enhanced using the edge detection function of "ImageJ". The green line is the shell's thickness projected into the focus plane.

3.2 Observation with the scanning electron microscope

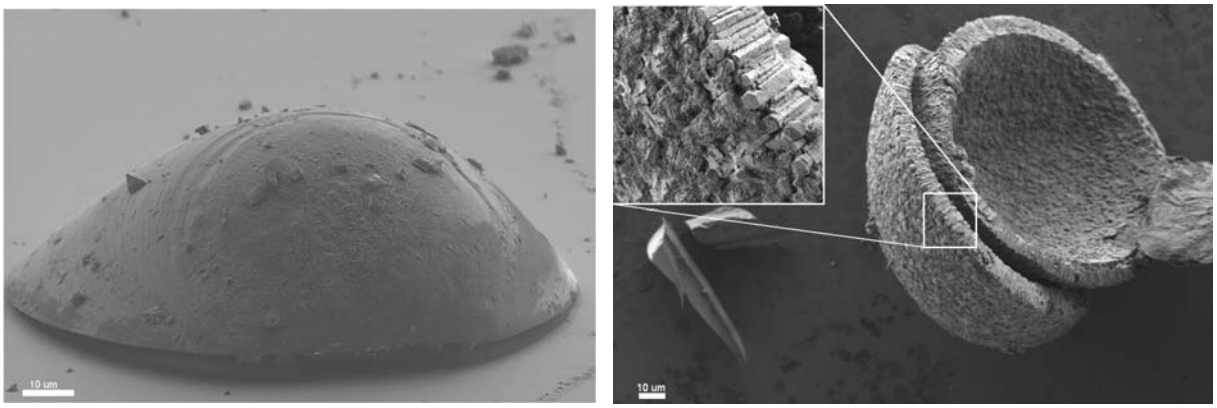

(A) **(B)**

Figure 7: (**A**) SEM image of the original shell does not give any hint about the crystallinity of the shell material. (**B**) SEM image of three-day old clamshells treated for epitaxial growth of calcium carbonate on their surfaces. The inset shows the morphologies of the epitaxially grown single crystals and their alignment revealing the structure of the original bio-crystals in the shell.

The shell of *Mercenaria mercenaria* (hard clamshell) is mineralized by aragonitic crystals which nucleate and grow in an organic matrix (Wilbur and Watabe, 1963; Taylor et al., 1973; Thorn et al., 1995). The formation of the organic matrix and nucleation of the aragonitic crystals control their orientation with respect to the overall shape of the shell (Tiwari and Gallager, 2003), thus controlling the shell's optical properties. To reveal the type and orientation of crystals inside the shell, we induced epitaxial growth of calcium carbonate crystals on the surface of shells, as described in section 2.2. This experiment was inspired by the work of Okazaki and Inoué on sea urchin spicules (Okazaki and Inoué, 1976). **Figure 7** shows SEM images of an untreated shell, and a shell with epitaxial growth of calcium carbonate crystals. In **Figure 7A**, the image of the original shell does not provide any clue about the type

and orientation of crystals inside the hard clamshell, while their morphology and alignment are shown clearly in **Figure 7B**. In particular, we can observe the pseudo-hexagonal morphology of crystals that were seeded by the crystalline material inside the shell. This morphology is compatible with an aragonitic crystal type for the hard clamshell (Bragg, 1924b; de Leeuw and Parker, 1998). In addition, the more important observation here is that the long axes of the pseudo-hexagonal crystals seem to be aligned perpendicular to the surface of the shell. Since the long axis is also the optic axis of the birefringent aragonite crystal (Bragg, 1924b), we expect the optic axis of the shell material to be nearly perpendicular to the shell's surface.

3.3 Analysis of the optic axis of clamshells using light field LC-PolScope

Aragonite is a negatively birefringent, biaxial crystal in which the three refractive indices for light polarized along the principal crystallographic axes are different from each other: $n_\gamma = 1.530$, $n_\alpha = 1.686$ and $n_\beta = 1.681$. The acute bi-sectrix is parallel to the crystallographic c-axis and is an axis of pseudo-hexagonal symmetry (Bragg, 1924a). Because the two higher refractive indices are almost equal and significantly higher than the third index value, the angle between the two optic axes is small (18 degrees) and the axes are nearly parallel to the crystallographic c-axis. Moreover, based on the epitaxial growth experiments with results shown in **Figure 7**, we expect the crystallographic c-axis to be perpendicular to the surface of the shell. The crystallographic a- and b-axes, however, do not seem to be aligned to each other throughout the thickness of the shell, giving the shell material the appearance of a uniaxial birefringent crystal in our optical experiments. Therefore, we approximate the shell material as a uniaxial crystal with $n_o = 1.530$, $n_e = (1.686 + 1.681)/2 = 1.684$, $\Delta(n)$

= n_o - n_e = -0.154, and the optic axis parallel to the pseudo-hexagonal or long axis of the aragonite crystals (Bragg, 1924a).

Since the LC-PolScope equipped with a standard camera only measures the 2D projection of the 3D optical anisotropy, it is not capable of determining the inclination angle of the optic axis of birefringent materials. To reveal the optic axis orientation, we recorded light field images of the same shell at different focus planes and present the images in **Figure 8**. The aperture images behind each microlens clearly reveal the orientation of the optic axis by mapping the retardance as a function of the tilt angle of rays passing through the shell material at each microlens location.

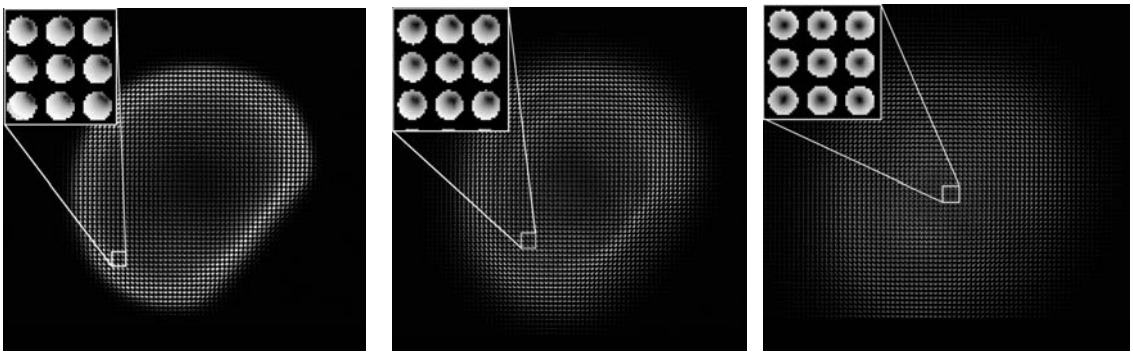

Bottom focus plane Middle focus plane Top focus plane

Figure 8: Light field retardance images with the nominal focus plane near the bottom, middle and top of the shell. The insets in the top left corners are magnified aperture images projected by an array of 3x3 microlenses chosen from shell regions that are in the respective focus plane and correspond to locations marked A_1 to A_3 in **Fig. 5**. The aperture images illustrate the incremental translocation of the retardance minimum to the edge of the aperture, caused by the increasing tilt of the optic axis away from the microscope axis. The magnified images are contrast enhanced.

For example, in **Figure 8**, the light field image with the focal plane near the top of the shell and its inset of aperture images demonstrate that rays focused in the center of the aperture carry no retardance, while rays focused near the edge of the aperture carry significant retardance. This clearly reveals the optic axis of the shell material at that location as being parallel to the microscope axis. Aperture images recorded at lower focus planes and picked from shell regions that are in focus demonstrate the gradual tilt of the optic axis away from the microscope axis as the shell bends downwards.

For a more quantitative evaluation, we establish the formula to calculate the retardance of a hard clamshell. The total retardance picked up by a ray passing through a uniaxial birefringent sample is determined by three factors: (1) The angle between the ray direction and the optic axis, (2) the physical path length of the ray inside the sample, and (3) the sample's birefringence (n_e - n_o).

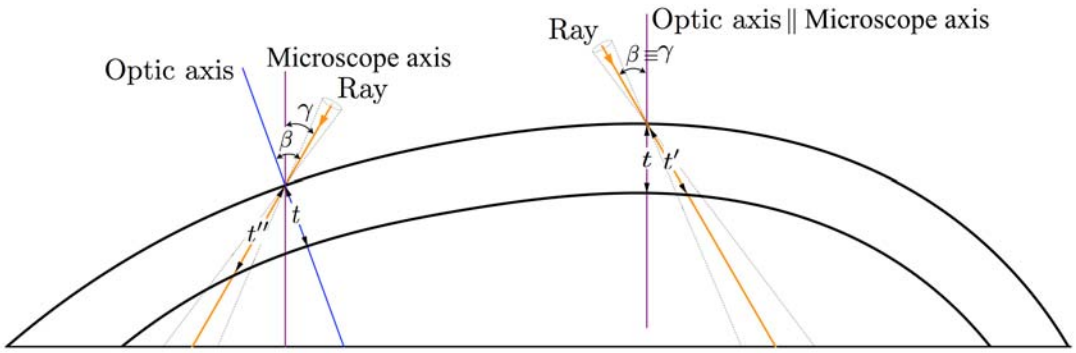

Figure 9: Sketch of a juvenile clamshell illustrating the relationship among the optic axis, the light ray and the microscope axis. The optic axis is assumed to be parallel to the normal of the shell with thickness t; t' and t" are physical path length of the ray at considered points.

For a sheet like material such as the shell, the retardance Δ imparted on a ray after passing through the sheet is determined by:

$$\Delta = \frac{t}{\cos\varepsilon}(n_e - n_o)\sin^2\beta \qquad [1]$$

where *t* is the thickness of the sheet, ε is the angle of the ray with respect to the normal of the sheet, and β is the angle between the ray and the optic axis. The term t/cos ε refers to the physical path length that increases with the tilt angle between the ray and the normal to the sheet, while the term $(n_e - n_o)\bullet\sin^2\beta$ refers to the increase in birefringence as the ray direction tilts away from the optic axis. In the special case where the optic axis is perpendicular to the shell surface (**Fig. 9**), the angles β and ε are equal, and equation (1) can be rewritten as:

$$\Delta = \frac{t}{\cos\beta}(n_e - n_o)\sin^2\beta \qquad [2]$$

In a microscope, ray directions in object space are described by the ray's tilt angle γ with respect to the microscope axis and its azimuth angle θ in the focus plane. The geometric relationship between the angles β, γ, θ, and the inclination angle σ and azimuth angle Φ of the optic axis leads to an expression for cos β that was first worked out by Oldenbourg (2008):

$$\cos\beta = \cos\theta\cos\sigma\cos\phi\sin\gamma + \cos\gamma\sin\sigma + \cos\sigma\sin\gamma\sin\theta\sin\phi \qquad [3]$$

The retardance patterns in aperture images such as shown in the insets of **Figure 8** can be subjected to a fitting procedure to estimate the parameters of shell thickness, inclination and azimuth angles. In a first step, we calibrated the aperture images that are projected by the microlenses onto the camera sensor in terms of the tilt angle γ of

a ray in object space and its radius position in the aperture image (see the supplemental information). Then we modeled the retardance pattern in the aperture by relating aperture positions (r, θ) to ray directions (γ, θ) in object space, the sheet thickness t, its birefringence (n_e - n_o), and optic axis orientation (σ, Φ). Using non-linear regression, we varied and found optimal values for the three parameters (σ, ϕ, t) until the simulated retardance images represented a best match with the experimental retardance patterns of selected aperture images. **Figure 10** shows the experimental and simulated retardance of one aperture image at the top focus plane and middle focus plane of the shell. The fitting procedure yielded optimized parameters, (σ, ϕ, t)= (88°, 164° , 530 nm) and (68°, 247°, 450 nm). This result confirmed our previous observations that the optic axes of the crystals are perpendicular to the shell surface which are identified as points A_1 and A_3 in **Figure 5B.** After applying the fitting procedure on the 3x3 aperture images in the insets of Figure 8 at the top focus plane, we found similar inclination angles for adjacent sampled areas with an angular standard deviation of about 2°. This standard deviation is partially caused by statistical variations and partially caused by a systematic change in inclination angle of 1.4° due to the curvature of the clamshell. In addition, we averaged the clamshell thickness over the same 3x3 aperture images and found an average thickness of 533 ± 41 nm for this three-day old shell.

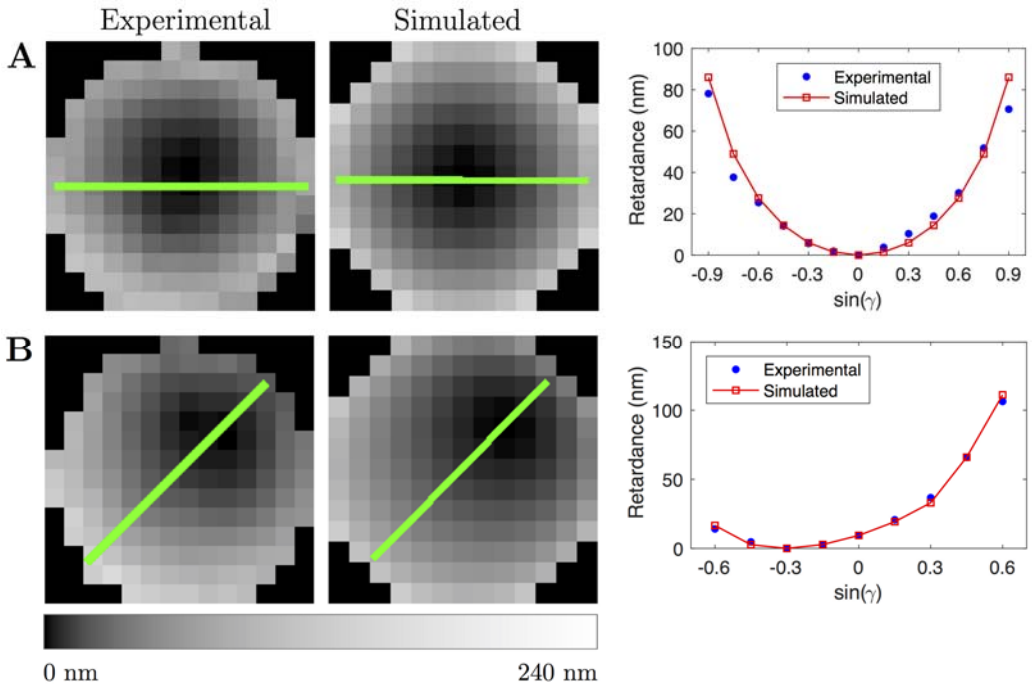

Figure 10: The experimental and simulated retardance conoscopic images and retardance profiles along green lines: (**A**) (σ, ϕ, t) = (88°, 164° , 530 nm); (**B**) (σ, ϕ, t) = (68°, 247°, 450 nm). The blue dots in the graphs represent experimental retardance values in angular steps of about 9°, the red lines represent simulated retardance values. In all four gray scale patterns, white represents 240 nm retardance and gray values are contrast enhanced using a logarithmic look-up-table.

The shell thickness derived from our retardance measurements is in good agreement with the thickness determined by the bright field method described in section 3.1. We then applied the same analysis to two-day and four-day old shells, compared their thicknesses near the top plane using both methods, and again found close agreement (see Table 1)

Shell's age	Polarized light field method	Conventional method
Two-day old	449± 42 nm	503 ±24 nm
Three-day old	533± 41 nm	594 ±20 nm
Four-day old	1157±167nm	1146 ±46 nm

Table 1: The thickness of shells of different age measured near the top plane using two methods.

From the data in **Table 1**, it is apparent that shell thickness increases moderately from day 2 to 3, but does so dramatically between day 3 and 4, and any older samples became too thick to be measured with the polarized light field method.

In **Figure 11** we show aperture images and line plots of retardance values measured for 2-, 3-, and 4-day old clamshells and wish to draw attention to the retardance measured in the minima located near the center of the aperture. As most apparent for the 4-day old clamshell, this retardance does not reach zero, but remains finite. This observation can be explained by the fact that the clamshell includes aragonite crystals which are biaxial crystals. Since the retardance of a single biaxial crystal has two minima in directions that are close to the crystallographic c-axis, and it seems that crystalline sub-regions in the shell are orientationally disordered around the c-axis, the retardance along directions near the c-axis never attain zero and remain finite because of the averaging within a resolved specimen volume. In thinner shells, this effect might be masked by the retardance sensitivity (~1nm) of our method or, more interestingly, might indicate a transition from a calcite to an aragonite crystal structure in nascent clamshells.

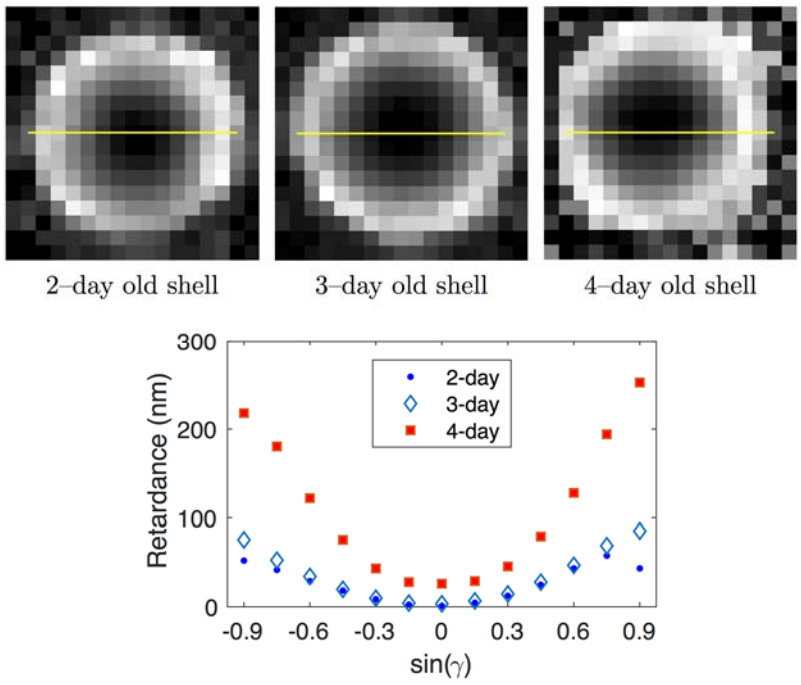

Figure 11: (**Top row**) The retardance aperture images of shells focused near their top plane with the darkest spot at the centers of the microlenses of two-day, three-day and four-day old clamshells, respectively. (**Bottom**) Plot profiles of retardance measured along horizontal yellow lines shown in top row illustrating the increase of retardance with age and the finite retardance (~30 nm) measured in the minimum of the 4-day old shell.

3.4 Diattenuation

We used the LC-PolScope to measure birefringence parameters of the clamshell material. The technique is known to be sensitive to diattenuation as well [Mehta, 2013]. Since there is measurable attenuation of the light that passes through the shell, as demonstrated by the bright field images in **Figs. 3, 4**, and **6**, we examined hard clamshells for diattenuation, i.e. polarization dependent attenuation that could affect our retardance measurements. Using a setup described by [Mehta, 2013] for measuring diattenuation, we found no measurable diattenuation in the shell material, except near the very edge of the shell, where some of the illumination and image rays propagate tangentially to the shell surface. Because diattenuation was confined to areas near the edge where grazing incidence is likely to cause polarization dependent scattering on surface roughness, the reported retardance values for more centrally located shell areas are not affected by diattenuation.

4. DISCUSSION

The work reported here is the first application of polarized light field microscopy to map the optic axis and birefringence of objects that have a true, three dimensional shape, unlike thin, straight calcite films, previously analyzed by this method [Oldenbourg, 2008]. Ultimately, our work is aimed at analyzing even more complex, three dimensional dynamic scenes using the same experimental setup and type of light field images, but paired with tomographic reconstruction algorithms. While clamshells represent three dimensional objects, the reconstruction of their birefringence parameters (optic axis and birefringence n_o - n_e) doesn't require tomographic approaches, because light rays that pass through the sample encounter only once a birefringent sheet. In more complex

structures, light rays that pass through the sample and contribute to the retardance and slow axis orientation measured in a given image point will usually traverse several structural elements that each have a different optic axis orientation and birefringence value. The current work aims to establish a simple model that can be used to develop and test more complex reconstruction algorithms. To simplify the current analysis of light field images further, we examined only those aperture images, which sampled the portion of the clamshell that was in the nominal focus plane in a given light field image. Furthermore, the aragonite crystal layers were approximated as a single uniaxial birefringent layer. Our results indicate that at a young age, this approximation holds well for clamshells

Our current polarization analysis of clamshell birefringence is built on ray optics, evaluating the retardance of rays that passed through the clamshell at different locations and at different inclination angles, as recorded in light filed images. This ray optic interpretation of light field images limits their spatial resolution to the size of a microlens (125μm) divided by the magnification of the objective lens (60x), equaling 2μm. Our results justify this approach, as the measured optic axis orientation, thickness, and birefringence of the clamshell varies smoothly and measurably only over longer distances.

In addition to establishing a test model for developing tomographic reconstruction algorithms for birefringence imaging, we hope that our results will facilitate the studies of shells in determining their morphology, especially their thickness as a function of age, and in revealing abnormalities in shell development during environmental stresses.

Ultimately, we work to extend the applications of our approach to structural studies in biology, physics, chemistry, medical and material science.

ACKNOWLEDGEMENTS

We are grateful for important contributions made by the following groups and individuals: the ARC hatchery in Dennis, MA for their generous provision of hard clam embryos; Dr. Scott Gallager of Woods Hole Oceanographic Institution (WHOI), Massachusetts, for invaluable comments and suggestions in the study of hard clamshells; the group of Prof. Levoy at Stanford University, especially Dr. Michael Broxton for generously sharing their 3D light field reconstruction program and kind support in installing, running and debugging the program; Amitabh Verma of the MBL for his prompt technical support; Louie Kerr of the MBL for helping with the SEM acquisition, and Talon Chandler for careful reading and suggestions for the manuscript. The work was supported by US federal grant GM114274 from the National Institute of General Medical Sciences.

REFERENCES

Bragg, W. (1924a). The refractive indices of calcite and aragonite. Proceedings of the Royal Society of London. Series A, Containing Papers of a Mathematical and Physical Character, 105(732):370– 386.

Bragg, W. (1924b). The structure of aragonite. Proceedings of the Royal Society of London. Series A, Containing Papers of a Mathematical and Physical Character, 105(729):16–39.

Broxton, M., Grosenick, L., Yang, S., Cohen, N., Andalman, A., Deisseroth, K., and Levoy, M. (2013). Wave optics theory and 3-D deconvolution for the light field microscope. Optics express, 21(21):25418–25439.

de Leeuw, N. H. and Parker, S. C. (1998). Surface structure and morphology of calcium carbonate polymorphs calcite, aragonite, and vaterite: an atomistic approach. The Journal of Physical Chemistry B, 102(16):2914–2922.

Levoy, M., Ng, R., Adams, A., Footer, M., & Horowitz, M. (2006, July). Light field microscopy. In ACM Transactions on Graphics (TOG) (Vol. 25, No. 3, pp. 924-934). ACM.

Mehta, S. B., Shribak, M., & Oldenbourg, R. (2013). Polarized light imaging of birefringence and diattenuation at high resolution and high sensitivity. Journal of Optics, 15(9), 094007.

Okazaki, K. and Inoué, S. (1976). Crystal property of the larval sea urchin spicule. Development, Growth & Differentiation, 18(4):413–434.

Oldenbourg, R. (2008). Polarized light field microscopy: an analytical method using a microlens array to simultaneously capture both conoscopic and orthoscopic views of birefringent objects. Journal of microscopy, 231(3):419–432.

Oldenbourg, R., S. Inoué, R. Tiberio, A. Stemmer, G. Mei and M. Skvarla. (1996). Standard test targets for high resolution light microscopy. In: H. C. Hoch, L. W. Jelinsky and H. Craighead, editors. Nanofabrication and Biosystems: Integrating Material

Science, Engineering and Biology. Cambridge, England: Cambridge University Press. p 123-138.

Oldenbourg, R. and M. Shribak. (2010). Microscopes. In: Michael Bass, Jay M. Enoch, Vasudevan Lakshminarayanan, Guifang Li, Carolyn Macdonald, Virendra N. Mahajan, Eric Van Stryland, editors. Handbook of Optics. 3rd ed. New York: McGraw-Hill, Inc. p 28.1 – 28.62.

Prevedel, R., Yoon, Y.-G., Hoffmann, M., Pak, N., Wetzstein, G., Kato, S., Schrödel, T., Raskar, R., Zimmer, M., Boyden, E. S., et al. (2014). Simultaneous whole-animal 3D imaging of neuronal activity using light-field microscopy. Nature methods, 11(7):727–730.

Taylor, J. D., Hall, A., and Kennedy, W. J. (1973). The Shell Structure and Mineralogy of the Bivalvia, [Part] II: Lucinacea-Clavagellacea Conclusions. Trustees of the British Museum, (Natural History).

Thompson, C. M., Hare, M. P., and Gallager, S. M. (2012a). Semi-automated image analysis for the identification of bivalve larvae from a Cape Cod estuary. Limnology and Oceanography: Methods, 10(7):538–554.

Thompson, C. M., York, R. H., and Gallager, S. M. (2012b). Species-specific abundance of bivalve larvae in relation to biological and physical conditions in a Cape Cod estuary: Waquoit Bay, Massachusetts (USA). Marine Ecology Progress Series, 469:53–69.

Thorn, K., Cerrato, R. M., and Rivers, M. L. (1995). Elemental distributions in

marine bivalve shells as measured by synchrotron X-ray fluorescence. The Biological Bulletin, 188(1):57–67.

Wilbur, K. M. and Watabe, N. (1963). Experimental studies on calcification in molluscs and the alga coccolithus huxleyi. Annals of the New York Academy of Sciences, 109(1): 82-112.